THE JOURNAL OF PHYSICAL CHEMISTRY C

Article

pubs.acs.org/JPCC

Theoretical Study on the Oxidation Mechanism and Dynamics of the Zigzag Graphene Nanoribbon Edge by Oxygen and Ozone

Kun Xu* and Peide D. Ye

School of Electrical and Computer Engineering and Birck Nanotechnology Center, Purdue University, West Lafayette, Indiana 47907, United States

Supporting Information

ABSTRACT: Graphene nanoribbons (GNRs), as an emerging class of material, hold great potential for the future high speed and low power electronic and spintronic devices. The fabrication of GNRs is of the utmost interest in terms of graphene based device research. Chemical narrowing of GNRs by oxidation is a promising technique in producing nanoribbons of desired widths. In this article, we hope to elucidate the etching mechanism of zigzag GNR (ZGNR) edge by oxidation through theoretical investigations. The oxidation mechanisms and dynamics of the ZGNR edge by O_2 and O_3 are fully revealed by density functional theory and statistical theory. The relationship between the reaction time and pressure as well as temperature is estimated dynamically. These theoretical results successfully interpret the recent experimental results and can be further used to predict the appropriate oxidation conditions for the precision etching of ZGNRs.

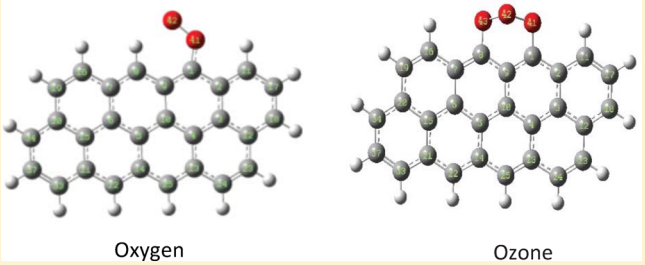

It is well-known that graphene has become the center of attention in the field of material research over the past decade.[1] The major milestones in graphene research led to the development of large area graphene sheets,[2] transparent electrodes,[3] and graphene based field effect transistors (FETs).[4] The high electron mobility of >15 000 $cm^2\ V^{-1}\ s^{-1}$ has been reported in ambient conditions.[1] Along with long spin diffusion length and relaxation times,[5] graphene is recognized as one of the most promising candidates for future electronic and spintronic devices. However, graphene is semimetallic without a bandgap. In order to overcome such a hurdle, attempts to open a bandgap have been made. Quantum confinement by narrowing graphene into nanoribbons allows the creation of a bandgap in the orders of the tenth of an eV.[6,7] Experimental results demonstrated the graphene nanoribbon (GNR) energy bandgap increases with reduced width.[8,9] It is crucial to fine-tune the techniques for the fabrication of GNRs to achieve the desired nanoribbon widths for specific bandgap openings.

For the two possible edge structures (zigzag and armchair), zigzag graphene nanoribbons (ZGNRs) possess localized nonbonding edge states,[10] in which every vertex carbon atom along the edge acts as a radical. Therefore, the edges of ZGNRs are prone to intense chemical activity. In recent experimental investigation with the electron spin resonance (ESR) measurements, Rao et al.[11] reported that the triplet state $O_2(^3\Sigma^-_g)$ can be adsorbed at the ZGNR edges easily at T = 300 K and P_{O2} = 1420 Torr. However, ZGNRs do not have the ability to adsorb many other gaseous molecules, such as H_2, N_2, He, and Ar. It is obvious that there is a particular interaction between ZGNRs and oxygen. Furthermore, Wang and Dai.[12] apply this particular property to narrow ZGNRs without damaging the basal plane of grapheme at high temperature, which can make the ZGNRs width to less than 10 nm. It becomes one of the important techniques[9,12−17] to obtain the ZGNRs with desired band gaps.

Nevertheless, despite several theoretical papers discussing this oxidation reaction published in recent years,[18−25] the oxidation reaction mechanism remains largely unclear. As this process occurs exclusively at the edge, we have conducted a systematical investigation aimed at unravelling the oxidation mechanisms of the edge carbon atom with oxygen and ozone and their dynamic features. We attempt to predict the etching rate ZGNRs by oxygen and ozone with high level of accuracy. It is hopeful that this study would enable much higher control for experimentalists who design fabrication processes to tailor the dimensions of ZGNRs.

COMPUTATIONAL METHODS

The geometric parameters of the stationary points on the oxidation reaction potential-energy surfaces of the ZGNR edge with O_2/O_3 were optimized by Gaussian 09 program[26] utilizing B3LYP functional[27] with 6-311G(d,p) and 3-21G(d) basis sets. For these solid−gas reaction systems, the critical parts concerning direct reaction atoms (High level) was calculated by the 6-311G(d,p) basis set and the other atoms (Low level) by the 3-21G(d) basis sets, which was performed by ONIOM method[28] implemented in Gaussian. The vibrational frequencies were calculated at all stationary points to determine the energy minimum structures and transition states. There is only

Received: January 19, 2014
Revised: April 23, 2014
Published: April 23, 2014

   dx.doi.org/10.1021/jp500633w | J. Phys. Chem. C 2014, 118, 10400−10407

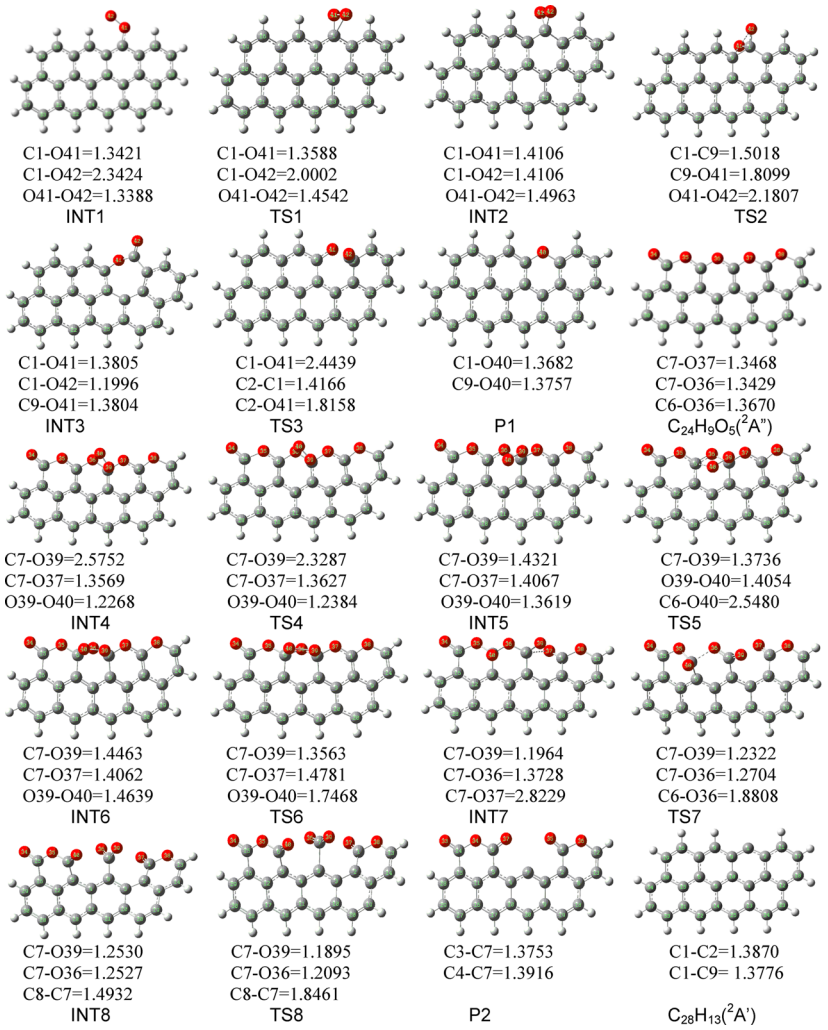

Figure 1. Main geometric parameters (bond lengths in Å) of intermediates (INT), transition states (TS), products (P), and $C_{28}H_{13}(^2A')$ for reaction (1).

one imaginary vibrational frequency for each one transition state.

The oxidation reaction rate constants were calculated by using the statistical mechanics and transition state rate theory in the *VARIFLEX* program.[29] The vibrational state densities were calculated by the direct state counting approach with the Beyer−Swinehart algorithm.[30] The contribution of both 3-translation and 3-dimenstion rotation were excluded for all stationary points except the gas phase molecule O_2 and O_3. The pressure dependence was treated by master equation using the Boltzmann probability of the complex. The potential energy path of the barrierless association process was approximated with the Morse potential function along the reaction coordinate in conjunction with the other two potentials, which are corresponding to the conserved and transitional degrees of freedom orthogonal to the reaction coordinate. The potential for the conserved degrees of freedom corresponds to the normal-mode vibrations in the separated fragments and is assumed to be the same as in the fragments. The potential for the transitional degrees of freedom is described in term of internal angles with sinusoidal functions.[31] The relationship of oxidation reaction time with the pressure of O_2 and O_3 was calculated by solving the rate differential equations. The details of the dynamical formulas are provided in Supporting Information.

RESULT AND DISCUSSION

Oxidation by O_2. In our other article,[32] we discussed the electronic spin state of the ZGNR edge and the alternating α and β spin configuration was considered as ground state of ZGNR. We can model ZGNR edge by $C_{28}H_{13}(^2A')$, as shown in Figure 1, to interact with $O_2(^3\Sigma^-_g)$, since only one oxygen atom of $O_2(^3\Sigma^-_g)$ can approach the edge carbon atom. Consequently, the initial oxidation of the outermost row carbon atoms of the ZGNR edge by oxygen molecules can be represented by the $C_{28}H_{13}(^2A')$ + $O_2(^3\Sigma^-_g)$ model reaction (denoted as reaction (1)). As shown in Figure 3, this reaction contains two low energy steps:

$$C_{28}H_{13}(^2A') + O_2(^3\Sigma^-_g) \rightarrow P1 + CO \quad (1a)$$

$$C_{24}H_9O_5(^2A'') + O_2(^3\Sigma^-_g) \rightarrow P2 + CO_2 \quad (1b)$$

The products, intermediates and transition states are denoted by the capital letters P, INT, and TS, respectively, in reaction (1). The main geometric parameters of these species calculated theoretically are all displayed in Figure 1 and their energies,

dx.doi.org/10.1021/jp500633w | J. Phys. Chem. C 2014, 118, 10400−10407

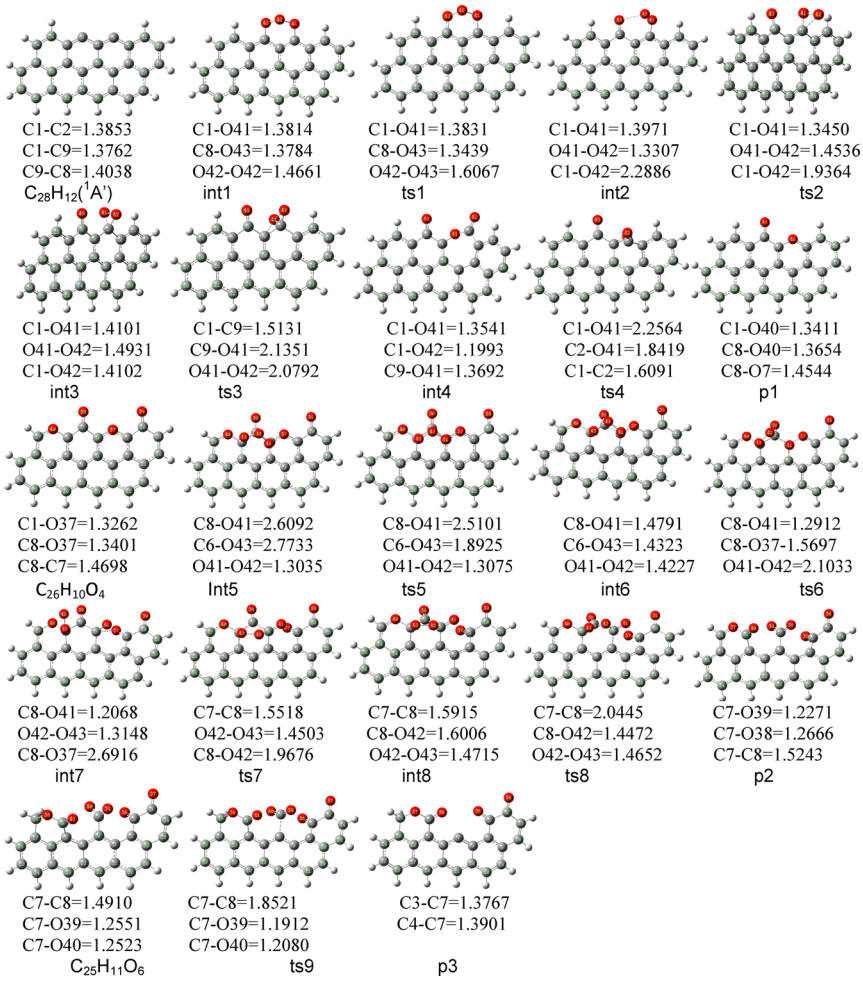

Figure 2. Main geometric parameters (bond lengths in Å) of intermediates (int), transition states (ts), products (p), and $C_{28}H_{12}(^1A')$ for reaction (2).

frequencies, and coordinates are listed in Table S1 of the Supporting Information in detail.

In reaction 1a, the adsorption complex INT1 is first formed with a C−O bond of 1.3421 Å and an adsorption energy of −45.2 kcal/mol, almost equal to the value of $C_{10}H_6(^1A') + O_2(^3\Sigma^-_g) \rightarrow C_{10}H_6O_2\ (^3A'')$ discussed in our other report,[32] which is in close agreement with −45.5 and −45.1 kcal/mol predicted by Park et al.[33] and Zhou et al.,[34] while it is higher than Sendt and Haynes's value (−32.3 kcal/mol)[24] in the doublet-$C_{22}H_9O_2 + O_2(^3\Sigma^-_g)$ system and lower than Silva-Tapia et al.'s result (−66.3 kcal/mol)[25] in the triplet-$C_{46}H_{16}O + O_2(^3\Sigma^-_g)$ system. Clearly, there is no reaction barrier in the combination of the carbon radical and the $O_2(^3\Sigma^-_g)$ molecule. The potential energy (V) versus the approaching distance (R) of C-OO can be described by a Morse function: $V(R) = 48.1\{1 - \exp[-4.064(R - 1.520)]\}^2$ kcal/mol.

In the adsorption complex (INT1), the dangling O atom behaves like an active radical. Comparing the elimination of the dangling O through the breaking of the O−O bond and the formation of a four-membered ring structure by attacking the C atom adjacent to the adsorbing C atom by the dangling O,[24] the lowest energy channel is the dangling O atom attacking the carbon atom of C-OO to form INT2 via a transition state (TS1) with a potential barrier of 17.1 kcal/mol. It is 7.1 kcal/mol lower than Sendt and Haynes's result[24] and in good agreement with Silva-Tapia et al.'s result.[25] The intermediate complex INT2 lies below INT1 by only 3.7 kcal/mol and can rearrange to the lower energy intermediate INT3 via transition state TS2 with a potential barrier of 11.5 kcal/mol by breaking the O−O bond and inserting one of the two oxygen atoms into the adjacent C−C bond while breaking the C−C bond. INT3 is a quite stable intra ester structure that sits 58.9 kcal/mol below INT2. Following the strong exothermicity of 110.4 kcal/mol from the reactants $C_{28}H_{13}(^2A') + O_2(^3\Sigma^-_g)$ to the intermediate INT3, the reaction can go through the transition state TS3 to produce P1 and CO with an exothermicity of 114.8 kcal/mol. Although TS3 is 63.7 kcal/mol higher than INT3, it is 46.7 kcal/mol below the $C_{28}H_{13}(^2A') + O_2(^3\Sigma^-_g)$ reactants and is the lowest transition state in energy. The new product P1 is formed by replacing the C atom of ZGNR edge with one oxygen atom.

In fact, each carbon radical of the ZGNR edge can absorb one oxygen molecule to form a P1-like product as discussed above. Therefore, the rational model cluster, $C_{24}H_9O_5\ (^2A'')$, with $O_2(^3\Sigma^-_g)$, can undergo a second oxidation step (1b). From a weak adsorption complex INT4 over a low barrier transition state TS4 to a slightly stronger adsorption complex INT5, the energy changes from −1.0 kcal/mol to −0.6 kcal/mol to −15.3 kcal/mol and the adsorption interatomic distance of O−C (labeled with C7−O39) shortens from 2.575 to2.329 Å to 1.432 Å. Next, the dangling O atom is easily absorbed by the neighboring C atom connecting the precursory oxygen

dx.doi.org/10.1021/jp500633w | J. Phys. Chem. C 2014, 118, 10400−10407

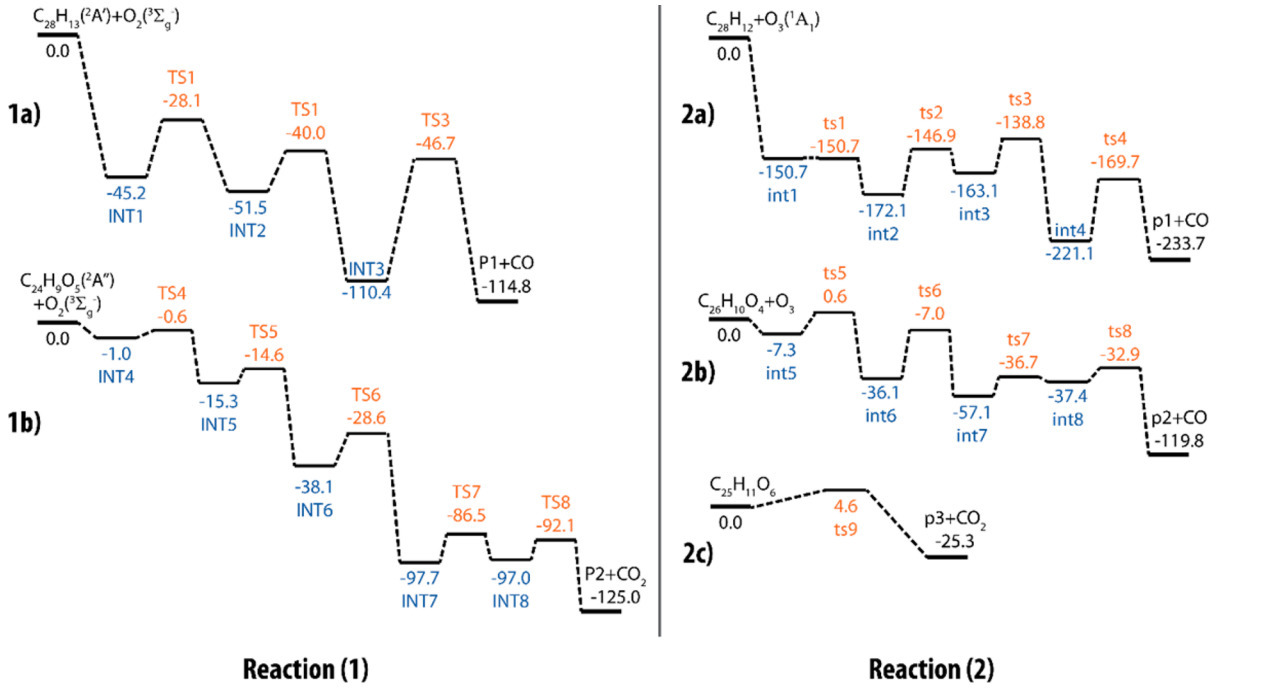

Figure 3. Potential energy surfaces of graphene edge with $O_2(^3\Sigma^-_g)$ and $O_3(^1A_1)$, in kcal/mol. (1a) and (1b) are the two low energy reaction steps for the initial oxidation of the outermost row carbon atoms of ZGNR edge by $O_2(^3\Sigma^-_g)$ (reaction (1)). (2a-c) represent the potential energy surface of the three reaction steps for the ozonolysis process of the ZGNR edge (reaction (2)).

atoms through the adsorption barrier of TS5, which is only 0.7 kcal/mol. The adsorption product INT6 is made up of a five-membered ring and sits below $C_{24}H_9O_5$ ($^2A''$) + $O_2(^3\Sigma^-_g)$ by 38.1 kcal/mol. INT6 is not stable enough because it can easily rearrange into the INT7 configuration via TS6 with much more exothermicity of 97.7 kcal/mol. This process goes over a barrier of only 9.5 kcal/mol with the separation of O−O and C−O bonds (O39−O40 and C7−O37). The rearranged complex (INT7) contains two intra ester structures and a tetrahedral carbon. The *tetra*−C-O- bond (labeled with C6−O36) of INT7 is easily broken via the transition state TS7 to form its isomer INT8, for which the forward and reverse barriers are 11.2 and 10.5 kcal/mol, respectively. However, from INT8, CO_2 is more readily eliminated with a low energy barrier of 4.9 kcal/mol via the transition state TS8. At the lowest energy, −125 kcal/mol, the products P2 and CO_2 complete in this reaction process.

From the P2 structure, we can see that there is a new carbon radical appearing at the vertex of the hexagon with the completion of reaction 1b. Apparently, with the all $-CO_2$ groups in the P2-like structure eliminated, the new ZGNR edge reappears and its width is reduced by 2.069 Å from the precursor ZGNR.

In light of the above oxidation mechanism of ZGNR edge with oxygen molecules, the reaction kinetic properties can be predicted by variational transition state theory with master equations. The temperature range is chosen to be from 300 to 2000 K and the pressure ranges from 0.01 Torr to 100 Torr. The result shows that there is a pressure effect only in the low temperature range of <500 K. In 300−500 K, the rate constant decreases with the increasing pressure and, because the rate constant is too small, the reaction would be dynamically very slow. Figure 4a illustrates the rate constants of reactions 1a and 1b with respect to reciprocal temperature at 1 Torr pressure. We observe that both rate constants increase rapidly with the increasing temperature from 300 K and reach the maxima at 800 K for k_{1a} and at 600 K for k_{1b}. Beyond the temperatures for the maximum rate constants, k_{1a} drops down slightly and k_{1b} keeps constant basically, while k_{1a} is several orders of magnitude higher than k_{1b} in high temperature range because reaction 1a is more favorable to proceed than reaction 1b. Therefore, reaction 1b is the rate-determining step. Also, the effects of the errors in energy barrier on the theoretical rate constant was checked for this reaction. At the temperature of 800 K and the pressure of 1 Torr, k_{1a} is predicted to be 2.61×10^{-11} cm^3 s^{-1}. With a given ±20% energy barrier error of the key transition state (TS1), k_{1a} are estimated to be 2.51×10^{-11} and 2.63×10^{-11} cm^3 s^{-1} at the TS1 energies of −24.7 and −31.5 kcal/mol. This signifies that the 20% error in barrier energy only causes a small change on the rate constant, because of the strong exothermic nature of the reaction and the positioning of the transition state below the reactants in energy. The same weak correlation between barrier energy and rate constant applies to k_{1b}, as well as reaction (2) discussed later in this report. Therefore, these theoretic results remain reliable despite any modest deviation in the reaction energy surface defined by density functional theory calculations.

To consider the appropriate reaction condition to avoid reacting too quickly or inefficiently, the dynamic properties of the $C_{28}H_{13}(^2A')$ + $O_2(^3\Sigma^-_g)$ model reaction were investigated. We varied the temperature over 500−1200 K and the O_2 pressure over 0.01−5 Torr, and solved the rate differential equations of reactions 1a and 1b. For one reaction cycle including the reactions 1a and 1b, two and a half carbon atoms (2.5C) of the ZGNR edge would be consumed with the release of CO and CO_2. Taking 2.5C as a reacting unit, the linear concentration of the ZGNR edge can be estimated to be 2.68×10^7 cm^{-1}. With the first row carbon atoms of ZGNR edge oxidized and the second row carbon atoms exposed, the oxidation reaction of the second row carbon atoms would start before the first row carbon atoms are completely oxidized. If

dx.doi.org/10.1021/jp500633w | J. Phys. Chem. C 2014, 118, 10400−10407

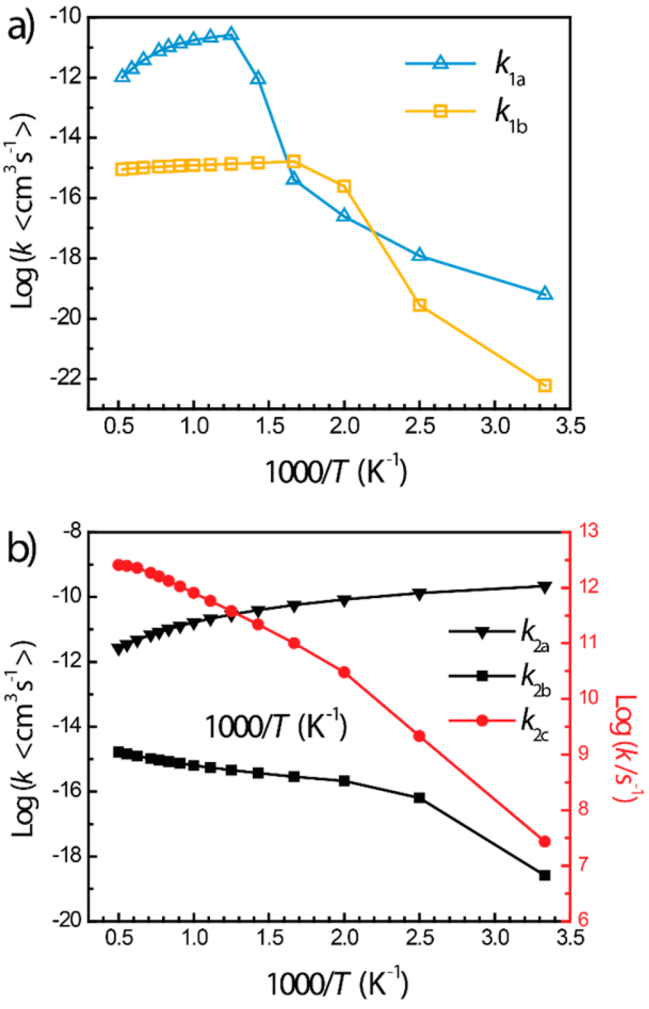

Figure 4. Rate constants of oxidation of ZGNR by (a) $O_3(^1A_1)$ and (b) $O_3(^1A_1)$ with respect to reciprocal temperature.

the first row carbon atom oxidation proceeds rapidly, the oxidation of the second row carbon atoms might occur with a slight delay. Figure 5A shows the predicted reaction time for the first row carbon atoms of ZGNR edge to be oxidized by 60%, 80%, and 99% at different temperatures and oxygen pressures. At a given temperature, there is a linear logarithm relationship between the reaction time and the oxygen pressure, in which the reaction time shortens with the increasing oxygen pressure. At any given oxygen pressure, the reaction time decreases with the increasing temperature and reaches the shortest time at 700 K. Above 700 K, the reaction time starts to lengthen continuously with increasing temperature, because k_{1a} decreases slightly at temperatures >800 K. Also, we can see that the lines in 700−1200 K are densely distributed. It shows the temperature influence on the reaction time is not as sensitive as oxygen pressure. In Wang and Dai's measurement[12] of graphene edge etching by O_2, the etching rates are about 3−5 nm/min at 1023 K and 0.1 Torr O_2 pressure and 3.8−5 nm/min at 1073 K and 0.025 Torr O_2 pressure. According to Figure 5A-c, at 1023 K and 0.1 Torr O_2 pressure the reaction time is estimated to be 4 s. The predicted etching rate should be 3.1 nm/min, which is consistent with the experimental value. Consequently, at oxygen pressure higher than 0.1 Torr the oxidation reaction of the second row carbon atom starts to proceed when the first row carbon atoms are approaching the point of depletion. As shown in Figure 5A-a, at 1073 K and 0.025 Torr O_2 pressure the reaction time is predicted to be 3.4 s. The predicted etching rate should be 3.7 nm/min, which is also close to the experimental result. At oxygen pressure lower than 0.025 Torr, the oxidation reaction of the second row carbon atom starts when the first row carbon atoms are 60% oxidized. The etching rate at 0.025−0.1 Torr may be predicted by Figure 5A-b, in which the oxidation reaction of the second row carbon atom begins to take place when the first row carbon atoms are 80% oxidized.

Oxidation by O_3. The ground state ozone molecule, $O_3(^1A_1)$, is of a diradical electronic configuration. There are two unpaired electrons with opposite spins at the two terminal oxygen atoms. These two oxygen atoms can simultaneously combine with two adjacent carbon radicals of ZGNR edge with little effort. Using the model of $C_{28}H_{12}(^1A')$ in Figure 2, the

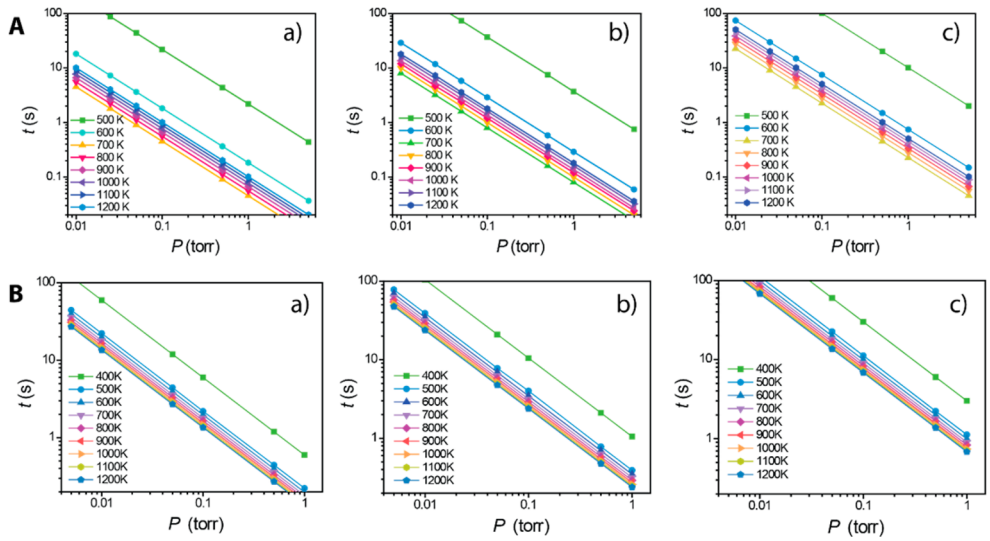

Figure 5. Reaction time of the oxidation of ZGNR edge. (A) The reaction time with respect to oxygen pressure. (B) The required time with respect to ozone pressure. (a), (b), and (c) represent 60%, 80%, and 99% of the outermost row carbon atoms of the ZGNR edge to be eliminated by oxidation.

dx.doi.org/10.1021/jp500633w | J. Phys. Chem. C 2014, 118, 10400−10407

ozonolysis mechanism contains three lowest energy steps as following

$$C_{28}H_{12}(^1A') + O_3(^1A_1) \rightarrow p1 + CO \quad (2a)$$

$$C_{26}H_{10}O_4(^1A') + O_3(^1A_1) \rightarrow p2 + CO \quad (2b)$$

$$C_{25}H_{11}O_6 \rightarrow p3 + CO_2 \quad (2c)$$

as shown in Figure 3, in which the intermediates, transition states, and products of reaction (2) are all designated in lower case, int, ts, and p, respectively, in order to distinguish them from reaction (1). The main geometric parameters of these stationary points are all displayed in Figure 2 and their energies, frequencies, and coordinates are listed in Table S2 of the Supporting Information in detailed.

In reaction 2a as shown in Figure 3, the first intermediate complex (int1) is formed barrierlessly from $C_{28}H_{12}(^1A')$ + $O_3(^1A_1)$ with an exothermic energy of 150.7 kcal/mol and two C−O bonds (labeled with C1−O41 and C8−O43) of about 1.38 Å. This barrierless process can be expressed by a Morse function: $V(R) = 156.2\{1 - \exp[-3.309(R - 1.500)]\}^2$ kcal/mol. Because of such a large association energy, the reverse reaction is difficult to occur under ambient conditions. However, the succeeding reaction from int1 to int2 proceeds with ease via the transition state ts1. The energy of ts1 is almost the same as that of int1, while int2 is 21.5 kcal/mol below int1. With the formation of int1, one O−O bond (labeled with O42−O43) elongates to 1.6067 Å and would break immediately transforming itself to int2, which has an active peroxy group like INT1 in the $C_{28}H_{13}(^2A')$ + $O_2(^3\Sigma^-_g)$ reaction. As a result, the dangling oxygen atom (O42) can make contact with the C atom (C1) to form a COO trigonal structure (int3) via the transition state ts2 with a barrier of 25.3 kcal/mol. The intermediate int3 is 163.1 kcal/mol below $C_{28}H_{12}(^1A')$ + $O_3(^1A_1)$ and it can be readily rearranged into an isomer int4, which is 221.1 kcal/mol below $C_{28}H_{12}(^1A')$ + $O_3(^1A_1)$, via the transition state ts3 with a barrier of 24.3 kcal/mol. Despite having undergone two transition states from int2, int4 can be formed promptly because both ts2 and ts3 are much lower than $C_{28}H_{12}(^1A')$ + $O_3(^1A_1)$ in energy. It can be seen that int4 contains the function groups of both ester (C−O−C═O) and quinine (C═O), which is consistent with the experimental result observed by Mawhinney et al.[35] in the oxidation of the rim of a single wall carbon nanotube with ozone. Then, int4 can decompose into products p1 and CO by the breaking of two bonds (C1−O4 and C1−C2) and the forming of another O−C bond (O41−C2) via the transition state ts4 with a barrier of 51.4 kcal/mol. The products p1 + CO are 233.7 kcal/mol below $C_{28}H_{12}(^1A')$ + $O_3(^1A_1)$. In addition, the oxidized product, p1, contains one C═O group and one C−O−C part. Therefore, with the completion of reaction 2a, both C═O and C−O−C groups can be formed alternately along the ZGNR edge.

Oxidized graphene corresponding to p1 can be represented by $C_{26}H_{10}O_4(^1A')$ for the second reaction step 2b. Combining with the second $O_3(^1A_1)$, a physic-adsorption complex (int5) can form with an exothermicity of 7.3 kcal/mol by electrostatic interaction between $C_{26}H_{10}O_4(^1A')$ and $O_3(^1A_1)$. Evidently, there is no barrier in the $C_{26}H_{10}O_4$ + $O_3(^1A_1)$ → int5 process. However, there is a transition state (ts5) between the physic-adsorption complex (int5) and the chemic-adsorption complex (int6). Since, ts5 is merely 0.6 kcal/mol higher than $C_{26}H_{10}O_4$ + $O_3(^1A_1)$ and int6 is 36.1 kcal/mol lower than $C_{26}H_{10}O_4$ + $O_3(^1A_1)$, the process of int5 → int6 could occur instantaneously with the 7.9 kcal/mol barrier. It is apparent that the O−O bond strength is weakened from O_3 molecule to int6. Following the formation of int6, the reaction further proceeds to a lower energetic intermediate int7 via transition state ts6 by breaking both O−O and C−O bonds (O41−O42 and C8−O37) simultaneously. The energies of ts6 and int7 are 7.0 and 57.1 kcal/mol below $C_{26}H_{10}O_4$ + $O_3(^1A_1)$. From int7, the active dangling O atom (O42) can attack the C atom (C8) of the C═O group to form the intermediate int8 through transition state ts7. The barrier of this process is 20.4 kcal/mol and int8 is only 0.7 kcal/mol lower than ts7. It is apparent that int8 is unstable. On one hand, the reversal from int8 to int7 can occur readily, on the other hand, with the breaking of the O−O bond (O43−O42) and two C−C bonds (C6−C7 and C7−C8), a forward decomposition leads to the more stable products p2 + CO via ts8 with the barrier of 4.5 kcal/mol. Since p2 + CO is also below $C_{26}H_{10}O_4$ + $O_3(^1A_1)$ by 119.3 kcal/mol, this decomposition is easy to take place.

From the above reaction 2b, one can find that the C−CO_2 bond (C7−C8) in p2 is stretched to 1.524 Å, which could enhance the CO_2 elimination and the new C radical formation (product p3) from p2. In order to keep the newly formed C radical from being contaminated by the surrounding O atoms, the doublet state $C_{25}H_{11}O_6$ is used to replace the singlet state p2 for investigate the following CO_2 elimination. We can see that, through the transition state ts9, reaction 2c undergoes the CO_2 elimination process and the elimination barrier is only 4.6 kcal/mol. This elimination produces stable CO_2 and the p3 radical, which are 25.3 kcal/mol lower than $C_{25}H_{11}O_6$. With the CO_2 eliminated on other sites, a new ZGNR edge is formed. Consequently, the ZGNR edge has been narrowed as the result of the consecutive reactions 2a, 2b, and 2c.

Figure 4b shows the predicted rate constants of the above three reaction steps in the temperature range of 300−2000 K. The rate constant (k_{2a}) of reaction 2a is in the ranges of about 1×10^{-10} to 2×10^{-12} cm^3/s and is negative temperature dependent because of its strongly exothermic and barrierless process, while the rate constant (k_{2b}) of reaction 2b is about 6−3 orders of magnitude less than k_{2a} and is positive temperature dependent. However, the rate constant (k_{2c}) of reaction 2c is strongly positive dependent on the temperature because of its small positive decomposition barrier. The reaction 2b is clearly the rate-determining step. It would cause excess concentrations of the intermediates and p1 of reaction 2a, especially in low temperature and at the beginning of the reaction. With the increasing temperature, the rate of reaction 2b increases to reduce the concentrations of the intermediates and p1 of reaction 2a. This explains Mawhinney and co-workers' experimental result,[35] which indicates that the infrared spectra of ester and quinone functional groups were observed at 298 K and begin to dwindle at 473 K and, then, completely disappear at 873 K.

On the basis of the rate constants and rate differential equations of reaction (2), the relationship of reaction time with respect to O_3 pressure is revealed in Figure 5(B). Because one reaction cycle may consume four carbon atoms (4C) of the ZGNR edge, the 1-dimensional concentration of the ZGNR edge can be assumed to be 2.01×10^7 cm^{-1} in terms of reaction unit 4C. Analogous to reaction (1), three plots represent the time-pressure relationship of the ozonolysis of the top row carbon atoms of ZGNR edge to 60%, 80%, and 99%. It can be seen that the ozonolysis time shortens with the increasing O_3

dx.doi.org/10.1021/jp500633w | J. Phys. Chem. C 2014, 118, 10400−10407

pressure. At a given O_3 pressure, the reaction time is very long at temperatures under 400 K because of limited value of k_{2b} at this temperature, while at 500 K the reaction time shortens dramatically because of the significant increase of k_{2b}. With further temperature increase, the reaction time still drops, but the change is much less significant. This implies that at high temperature the reaction time is not very sensitive to temperature change. In order to compare reaction (2) with reaction (1) dynamically, Figure 6 displays the change of

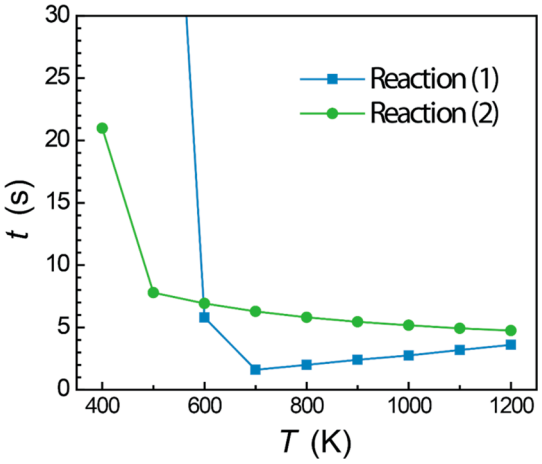

Figure 6. Required reaction time versus temperature at 0.05 Torr (O_2 or O_3) for 80% carbon atoms of top row of ZGNR edge to be eliminated by oxidation.

reaction time with respect to the temperature at the pressure of 0.05 Torr (O_2 or O_3) and the edge 80% oxidized. It is obvious that the reaction time of reaction (1) is much longer than that of reaction (2) at under 600 K because of the smaller k_{1a} and k_{1b}, while the former is somewhat shorter at above 600 K since k_{1b} is about a factor of 2 times greater than k_{2b}. At high temperature and low O_3 pressure, ozonolysis has a slightly longer reaction time, which is favorable to control the process of etching ZGNR edge. Therefore, ozone molecule might be a good oxidant like oxygen molecule for etching ZGNR edge.

CONCLUSION

In summary, the oxidation mechanisms of ZGNR edge by O_2 and O_3 have been studied by using density functional theory. The $C_{28}H_{13}(^2A')$ + $O_2(^3\Sigma^-_g)$ model reaction (1) is a consecutive two-step reaction and the $C_{28}H_{12}(^1A')$ + $O_3(^1A_1)$ model reaction (2) involves a consecutive three-step reaction. In the first reaction step, the exothermicity of reaction (1) is estimated to be 114.8 kcal/mol and that of reaction (2) is 233.7 kcal/mol. The rate-determining step is the second step for both reactions. The dynamic analysis shows that, for one row carbon atoms etching, the oxidation time shortens significantly with increasing O_2/O_3 pressure. For reaction (1), it shortens rapidly when the temperature increases from 400 to 700 K and lengthens slowly at temperatures higher than 700 K. For reaction (2), the reaction time at 400 K is very long, while at 500 K it shortens dramatically. At temperatures over 500 K, the reaction time continues to drop, but the change is much less significant. Therefore, the etching processes of ZGNR by the oxidation of O_2 and O_3 can be precisely controlled by temperature and pressure. Also, this theoretical result predicts the O_3 etching process can act as an excellent alternative to the existing O_2 process.

ASSOCIATED CONTENT

Supporting Information

Coordinates, frequencies, and energies of all stationary points of the oxidation reactions of ZGNR edge with oxygen molecules. This material is available free of charge via the Internet at http://pubs.acs.org.

AUTHOR INFORMATION

Corresponding Author

*E-mail: xu83@purdue.edu.

Notes

The authors declare no competing financial interest.

REFERENCES

(1) Geim, A. K.; Novoselov, K. S. The Rise of Graphene. *Nat. Mater.* **2007**, *6*, 183−191.

(2) Kim, K. S.; Zhao, Y.; Jang, H.; Lee, S. Y.; Kim, J. M.; Kim, K. S.; Ahn, J.-H.; Kim, P.; Choi, J.-Y.; Hong, B. H. Large-Scale Pattern Growth of Graphene Films for Stretchable Transparent Electrodes. *Nature* **2009**, *457*, 706−710.

(3) Bae, S.; Kim, H.; Lee, Y.; Xu, X.; Park, J.-S.; Zheng, Y.; Balakrishnan, J.; Lei, T.; Kim, H. R.; Song, Y. I.; et al. Roll-to-Roll Production of 30-Inch Graphene Films for Transparent Electrodes. *Nat. Nanotechnol.* **2010**, *5*, 574−578.

(4) Kedzierski, J.; Hsu, P.-L.; Reina, A.; Kong, J.; Healey, P.; Wyatt, P.; Keast, C. Graphene-on-Insulator Transistors Made Using C on Ni Chemical-Vapor Deposition. *Electron Device Lett., IEEE* **2009**, *30*, 745−747.

(5) Kim, W. Y.; Kim, K. S. Prediction of Very Large Values of Magnetoresistance in a Graphene Nanoribbon Device. *Nat. Nano* **2008**, *3*, 408−412.

(6) Barone, V.; Hod, O.; Scuseria, G. E. Electronic Structure and Stability of Semiconducting Graphene Nanoribbons. *Nano Lett.* **2006**, *6*, 2748−2754.

(7) Yang, L.; Park, C.-H.; Son, Y.-W.; Cohen, M. L.; Louie, S. G. Quasiparticle Energies and Band Gaps in Graphene Nanoribbons. *Phys. Rev. Lett.* **2007**, *99*, 186801.

(8) Son, Y.-W.; Cohen, M. L.; Louie, S. G. Energy Gaps in Graphene Nanoribbons. *Phys. Rev. Lett.* **2006**, *97*, 216803.

(9) Han, M. Y.; Özyilmaz, B.; Zhang, Y.; Kim, P. Energy Band-Gap Engineering of Graphene Nanoribbons. *Phys. Rev. Lett.* **2007**, *98*, 206805.

(10) Jiang, D.; Sumpter, B. G.; Dai, S. Unique Chemical Reactivity of a Graphene Nanoribbon's Zigzag Edge. *J. Chem. Phys.* **2007**, *126*, 134701−134701−6.

(11) Rao, S. S.; Stesmans, A.; Keunen, K.; Kosynkin, D. V.; Higginbotham, A.; Tour, J. M. Unzipped Graphene Nanoribbons as Sensitive O_2 Sensors: Electron Spin Resonance Probing and Dissociation Kinetics. *Appl. Phys. Lett.* **2011**, *98*, 083116−083116−3.

(12) Wang, X.; Dai, H. Etching and Narrowing of Graphene from the Edges. *Nat. Chem.* **2010**, *2*, 661−665.

(13) Tapasztó, L.; Dobrik, G.; Lambin, P.; Biró, L. P. Tailoring the Atomic Structure of Graphene Nanoribbons by Scanning Tunnelling Microscope Lithography. *Nat. Nano* **2008**, *3*, 397−401.

(14) Stampfer, C.; Güttinger, J.; Hellmüller, S.; Molitor, F.; Ensslin, K.; Ihn, T. Energy Gaps in Etched Graphene Nanoribbons. *Phys. Rev. Lett.* **2009**, *102*, 056403.

(15) Kosynkin, D. V.; Higginbotham, A. L.; Sinitskii, A.; Lomeda, J. R.; Dimiev, A.; Price, B. K.; Tour, J. M. Longitudinal Unzipping of Carbon Nanotubes to Form Graphene Nanoribbons. *Nature* **2009**, *458*, 872−876.

(16) Wu, Z.-S.; Ren, W.; Gao, L.; Liu, B.; Zhao, J.; Cheng, H.-M. Efficient Synthesis of Graphene Nanoribbons Sonochemically Cut from Graphene Sheets. *Nano Res.* **2010**, *3*, 16−22.

(17) Masubuchi, S.; Ono, M.; Yoshida, K.; Hirakawa, K.; Machida, T. Fabrication of Graphene Nanoribbon by Local Anodic Oxidation Lithography Using Atomic Force Microscope. *Appl. Phys. Lett.* **2009**, *94*, 082107−082107−3.
(18) Montoya, A.; Mondragón, F.; Truong, T. N. First-Principles Kinetics of CO Desorption from Oxygen Species on Carbonaceous Surface. *J. Phys. Chem. A* **2002**, *106*, 4236−4239.
(19) Frankcombe, T. J.; Smith, S. C. On the Microscopic Mechanism of Carbon Gasification: A Theoretical Study. *Carbon* **2004**, *42*, 2921−2928.
(20) Sendt, K.; Haynes, B. S. Density Functional Study of the Reaction of Carbon Surface Oxides: The Behavior of Ketones. *J. Phys. Chem. A* **2005**, *109*, 3438−3447.
(21) Radovic, L. R.; Bockrath, B. On the Chemical Nature of Graphene Edges: Origin of Stability and Potential for Magnetism in Carbon Materials. *J. Am. Chem. Soc.* **2005**, *127*, 5917−5927.
(22) Veiga, R. G. A.; Miwa, R. H.; Srivastava, G. P. Quenching of Local Magnetic Moment in Oxygen Adsorbed Graphene Nanoribbons. *J. Chem. Phys.* **2008**, *128*, 201101−201101−3.
(23) Radovic, L. R. Active Sites in Graphene and the Mechanism of CO_2 Formation in Carbon Oxidation. *J. Am. Chem. Soc.* **2009**, *131*, 17166−17175.
(24) Sendt, K.; Haynes, B. S. Density Functional Study of the Reaction of O_2 with a Single Site on the Zigzag Edge of Graphene. *Proc. Combust. Inst.* **2011**, *33*, 1851−1858.
(25) Silva-Tapia, A. B.; García-Carmona, X.; Radovic, L. R. Similarities and Differences in O2 Chemisorption on Graphene Nanoribbon vs. Carbon Nanotube. *Carbon* **2012**, *50*, 1152−1162.
(26) Frisch, M.; Trucks, G.; Schlegel, H.; Scuseria, G.; Robb, M.; Cheeseman, J.; Scalmani, G.; Barone, V.; Mennucci, B.; Petersson, G.; et al. *Gaussian 09*, revision B.01; Gaussian, Inc.: Wallingford CT, 2009.
(27) Becke, A. D. Density-functional Thermochemistry. III. The Role of Exact Exchange. *J. Chem. Phys.* **1993**, *98*, 5648−5652.
(28) Dapprich, S.; Komáromi, I.; Byun, K. S.; Morokuma, K.; Frisch, M. J. A New ONIOM Implementation in Gaussian98. Part I. The Calculation of Energies, Gradients, Vibrational Frequencies and Electric Field Derivatives. *J. Mol. Struct.: THEOCHEM* **1999**, *461*−*462*, 1−21.
(29) Klippenstein, S. J.; Wagner, A. F.; Dunbar, R. C.; Wardlaw, D. M.; Robertson, S. H. *VARIFLEX Version 1.00*; Argonne National Laboratory, 1999.
(30) Beyer, T.; Swinehart, D. F. Algorithm 448: Number of Multiply-Restricted Partitions. *Commun. ACM* **1973**, *16*, 379.
(31) Miller, J. A.; Klippenstein, S. J.; Robertson, S. H. A Theoretical Analysis of the Reaction between Ethyl and Molecular Oxygen. *Proc. Combust. Inst.* **2000**, *28*, 1479−1486.
(32) Xu, K.; Ye, P. D. *Electron Spin Magnetism of Zigzag Graphene Nanoribbon Edge States*, submitted.
(33) Park, J.; Xu, Z. F.; Lin, M. C. Kinetic Study of the $C_{10}H_7 + O_2$ Reaction. *J. Phys. Chem. A* **2009**, *113*, 5348−5354.
(34) Zhou, C.-W.; Kislov, V. V.; Mebel, A. M. Reaction Mechanism of Naphthyl Radicals with Molecular Oxygen. 1. Theoretical Study of the Potential Energy Surface. *J. Phys. Chem. A* **2012**, *116*, 1571−1585.
(35) Mawhinney, D. B.; Naumenko, V.; Kuznetsova, A.; Yates, J. T.; Liu, J.; Smalley, R. E. Infrared Spectral Evidence for the Etching of Carbon Nanotubes: Ozone Oxidation at 298 K. *J. Am. Chem. Soc.* **2000**, *122*, 2383−2384.